Simplified Device Simulation of Silicon Solar Cells Using a Lumped Parameter Optical Model

Andreas Fell, Keith R. McIntosh, and Kean C. Fong

***Abstract*—An optical model for solar cell device simulations providing a computational rapid alternative or extension to ray tracing is presented. Its lumped input parameters are mainly the wavelength-dependent external front surface transmission T_{ext} and pathlength enhancement Z, which can be derived by measurements and/or ray tracing of finished devices. A way to calculate the generation profile G from those inputs is described, showing negligible error for typical silicon solar cell properties compared to G from ray tracing. Including a recently proposed parameterization of Z, it is shown that the lumped input parameters are, to good approximation, independent of 1) the incident spectrum, 2) the device thickness, and 3) the device temperature. The latter mainly assumes that the temperature influence of the silicon bulk dominates over the thin film's one, which is shown experimentally for a few typical thin-film materials. The model is successfully applied to accurately predict optical characteristics of high efficiency laboratory solar cells with two different thicknesses and temperatures. It is thus useful to simplify and speed up optical modeling relative to ray tracing alone, without significant error for typical silicon solar cell properties.**

***Index Terms*—Modeling, optics, Quokka, silicon, simulation, solar cell, temperature coefficient.**

I. Introduction

CALCULATING the generation profile is an essential part of modeling a crystalline silicon solar cell. For a given spectral irradiation, the generation profile essentially depends on the optical and geometrical properties of the materials. These are the thickness and wavelength-dependent complex refractive index of the silicon and of any dielectric and metallic films, as well as the surface morphology of the solar cell.

A detailed and practical approach to optical modeling combines the transfer matrix method (TMM) to account for thin-film effects with geometrical ray tracing within the silicon. Drawbacks of this approach are 1) its significant computational demand and 2) inaccuracies arising from poorly known material properties and from the treatment of complicated surface morphologies by simpler geometrical shapes required for ray tracing.

When the above complications are prohibitive or when rapid solutions are required, simpler models that use lumped characteristics of the device as inputs (rather than material properties) can be employed. Lumped input parameters can be, for example, the front reflection, which is directly measurable on a finished cell.

The most widely used optical model using lumped input parameters is the "Basore model" [1], [2], which was extended in [3]. It omits detailed modeling of thin-film effects by using the transmission through the front surface T_{ext} as a lumped input parameter. It analytically, and therefore rapidly, calculates internal reflections in a simplified but still physically meaningful way, using several more input parameters. It was shown to be reasonably accurate, even for textured surfaces, but typically still requires fitting of some input parameters to achieve good agreement with the generation current derived from ray tracing or with measured cell characteristics [4].

In this study, a simplification of the Basore model is investigated, using the pathlength enhancement factor Z as a single (wavelength-dependent) lumped parameter to represent internal optics. As a further simplification, a recently proposed parameterization of Z is included in the investigations, which provides the particular benefit of its parameters being independent of device thickness [5]. Together with the lumped parameter T_{ext}, this constitutes a minimal approach to spectrally resolved optical modeling. The model can be used to derive the generation profile from optical measurements of a finished device, as well as a second step to ray tracing, which readily outputs those lumped parameters with less effort than the generation profile.

The basic description of this model and initial comparisons with ray tracing have been published in [6]. This paper extends the validation of the model by investigating the accuracy of quantum efficiency simulations.

A second extension is an evaluation of the temperature dependence of the lumped input parameters. Theoretical considerations suggest that their functional dependence on the silicon absorption coefficient is, to good approximation, independent of temperature for nonhighly absorbing wavelengths. For shorter wavelengths on the other hand, the wavelength-dependence can be considered to be temperature-independent. This means that once a unique set of input parameters is derived for a particular cell, the model is able to correctly account for the influence of temperature on the generation profile. The main underlying assumption of temperature-independent properties of thin films is tested experimentally for a few common

Manuscript received November 21, 2015; revised November 30, 2015; accepted February 2, 2016. The work of A. Fell was supported by the Australian Government through the Australian Renewable Energy Agency under the Fellowship 5-F007.

A. Fell was with the Australian National University, Canberra, ACT 0200, Australia. He is now with the Fraunhofer Institute for Solar Energy Systems, Freiburg 79110, Germany (e-mail: andreas.fell@ise.fraunhofer.de).

K. R. McIntosh is with PV Lighthouse, Wollongong, NSW 2500, Australia (e-mail: krmcintosh@pvlighthouse.com.au).

K. C. Fong is with the Australian National University, Canberra, ACT 0200, Australia (e-mail: kean.fong@anu.edu.au).

Color versions of one or more of the figures in this paper are available online at http://ieeexplore.ieee.org.

Digital Object Identifier 10.1109/JPHOTOV.2016.2528407

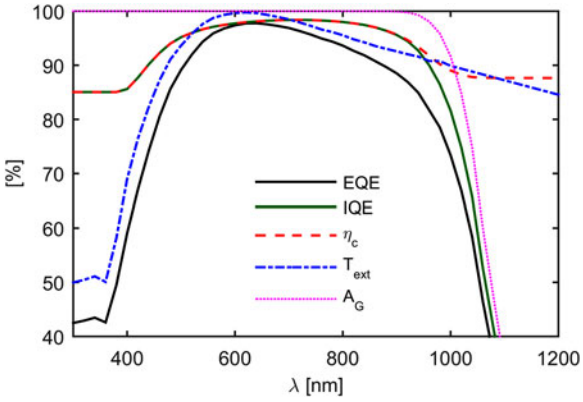

Fig. 1. Example of spectral optical parameters typical for a silicon solar cell (conventional cell from [7], no metal shading).

materials via reflection measurements on polished samples. Other simplifying assumptions are tested against ray tracing.

Finally, the model is applied to predict the quantum efficiency of laboratory interdigitated-back-contact (IBC) solar cells for varying device thickness and temperature.

II. Theory

A. Definition of Optical Parameters

Fig. 1 illustrates the main spectral optical parameters of a typical silicon solar cell, which influence the measurable external quantum efficiency EQE. Its integration over the incident spectral intensity I determines the short-circuit current density J_{SC}

$$J_{\mathrm{SC}} = q \int_0^\infty I(\lambda)\, EQE(\lambda)\, d\lambda. \tag{1}$$

The EQE can be factored into three properties: 1) the transmission of incident photons through the front surface T_{ext} (including front film absorption A_{front}), 2) the fraction of transmitted photons generating electron hole pairs via band-to-band absorption A_G, and 3) the electrical quality of the device to collect the generated carriers, quantified by the collection efficiency η_c

$$EQE(\lambda) = T_{\mathrm{ext}}(\lambda)\, A_G(\lambda)\, \eta_c(\lambda). \tag{2}$$

A_G is related to the pathlength enhancement factor Z, the absorption coefficient of silicon α, and the device thickness W by [1]

$$A_G(\lambda) = 1 - \exp(-\alpha(\lambda)\, Z(\lambda) W). \tag{3}$$

The internal quantum efficiency IQE is defined by

$$IQE(\lambda) = A_G(\lambda)\, \eta_c(\lambda). \tag{4}$$

Note that this definition corresponds to "IQE_{LT}" in [1], opposed to the often applied definition $T_{\mathrm{ext}} = 1 - R_{\mathrm{Total}}$, which neglects A_{front}, and includes the escape reflection in the measureable total reflection R_{Total}. While the latter definition is experimentally more easily applied, the former is preferred in this study to better differentiate these effects for device modeling.

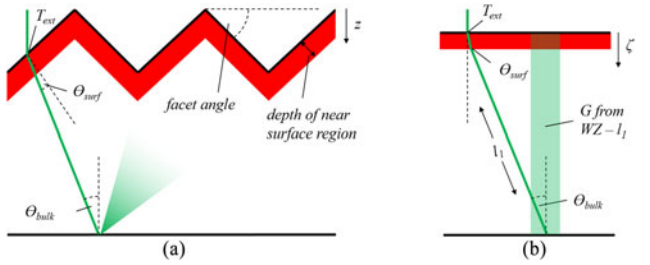

Fig. 2. This paper's model indicating the path of a ray for: 1) assumed (textured) surface and 2) its representation in a quasi-1-D domain with a planar surface wherein the generation profile is calculated.

The scope of this study is to model the generation for subsequent electrical device simulation, which then accounts for the carrier collection. The total generation current J_G consequently differs from J_{SC} by excluding η_c and can be expressed as

$$J_G = q \int_0^\infty I(\lambda)\, T_{\mathrm{ext}}(\lambda) \left(1 - \exp(-\alpha(\lambda)\, Z(\lambda) W)\right) d\lambda. \tag{5}$$

Equation (5) highlights that J_G, and its spectrally resolved contributions, are defined by the two parameters T_{ext} and Z, for given α, W, and I.

B. Calculating the Generation Profile

The approach to calculate the generation profile $G(\zeta)$ is based on [2], [3], and [8], which accounts for different path angles in the near-surface region (e.g., the depth of a p-n junction) and the bulk, θ_{surf} and θ_{bulk}, by a faceted-surface model. It is comprehensively summarized in [4]. Notably, ζ represents the closest distance to the (textured) front surface rather than the depth coordinate z, and it is best suited to defining the 1-D generation profile required for electrical modeling with the simplification of a planar front surface.

A schematic overview of this paper's model is shown in Fig. 2. It is identical to the one described above for the first pass of a ray to the rear surface with a travel length l_1, resulting in the first-pass generation profile $G_1(\zeta, \lambda)$. However, subsequent internal rays are not modeled explicitly, as Z does not provide information on internal reflectance or reflected path angles. Instead, the generation from the remaining pathlength $ZW - l_1$ is evenly distributed over the entire cell thickness

$$\begin{aligned} G(\zeta, \lambda) \;=\; & G_1(\zeta, \lambda) + W^{-1} I(\lambda)\, T_{\mathrm{ext}}(\lambda) \left(\exp(-\alpha(\lambda)\, l_1)\right. \\ & \left. - \exp(-\alpha(\lambda)\, Z(\lambda) W)\right). \end{aligned} \tag{6}$$

C. Deriving T_{ext} and Z

Deriving T_{ext} and Z from ray tracing is straightforward with most existing software tools. It notably demands much less computational effort than to calculate the generation profile, which requires discretization of the silicon bulk region.

T_{ext} and Z can also be derived from EQE and total reflection R_{Total} measurements. Essentially, the influence of only indirectly measurable optical (front film absorption A_{front} for short

wavelengths and $1 - A_G$ for long wavelengths) and electrical losses (η_c) on the measured quantum efficiency must be deconvolved.

For short wavelengths, A_{front} may be significant, and is often not considered explicitly but lumped into η_c. This results in an overestimation of generation and an underestimation of IQE, which compensate to match the measured EQE. Whether this simplification is acceptable depends on the level of insight required for the device modeling task.

For long wavelengths, it is possible to deconvolve Z and η_c via the inverse IQE [1], [2]. Alternatively, often an assumption for η_c can be made so that Z can be derived from the IQE via (3) and (4) (see [9]). Within opto-electrical modeling of a particular solar cell, electrical device properties (which define η_c) and Z can be uniquely fitted to match both electrical and optical cell characteristics.

D. Z Parameterization

A parameterization to describe the wavelength dependence of Z was derived in [5]

$$Z(\alpha) = Z_\infty + \frac{1}{\alpha Z_p W} \ln\left[\frac{Z_0}{Z_\infty} - \left(\frac{Z_0}{Z_\infty} - 1\right)\exp\left(-\alpha Z_\infty Z_p W\right)\right]. \quad (7)$$

The main assumptions for its analytical derivation are that the average transmission angle and the internal reflectances are wavelength independent. This was shown in [5] to not introduce significant error by accurately fitting (8) to ray tracing results for a variety of typical solar cell properties.

To determine the Z parameters, (7) is fitted to a known Z. It was found that restricting the fitting range to 0.6 cm^{-1} $< \alpha <$ 60 cm^{-1}, which is the range where Z has a significant influence on device characteristics, gives the best overall accuracy. If fitting is not directly performed to $Z(\alpha)$ but indirectly to $Z(\lambda)$, it is important to consistently use the same data for $\alpha(\lambda)$ as assumed for the derivation of $Z(\lambda)$.

E. Temperature Independence of T_{ext} and Z

For the typical operating conditions of silicon solar cells (approximately -50 to 80 °C), the optical property that shows by far the largest temperature dependence is the absorption coefficient of silicon α. The optical properties of typical dielectric and metallic thin films used in silicon solar cells are therefore assumed to be approximately temperature independent.

A change in α mainly impacts the internal light trapping, i.e., the input parameter Z. Based on the same assumptions as in the previous section, Z is primarily a function of α, which is the only wavelength- and temperature-dependent parameter. This means that once $Z(\alpha)$ is determined, it can be assumed to be temperature independent, and $Z(\lambda, T)$ can be calculated for any temperature T by a known $\alpha(\lambda, T)$. Notably, the three Z parameters Z_0, Z_∞ and Z_p are independent of α and can therefore be assumed to be temperature independent as well.

To a lesser but potentially still significant extent, T_{ext} can be affected by changes in α due to its influence on the interface reflection. However, for highly absorbing wavelengths, α is only weakly dependent on temperature, and the dielectric film properties typically introduce a strong wavelength dependence of T_{ext}. At lowly absorbing wavelengths on the other hand, the influence of the dielectric films on the wavelength dependence is decreased, and α dominates the temperature and wavelength dependence. Therefore, temperature independence of $T_{\mathrm{ext}}(\lambda)$ for $\lambda < 900$ nm and of $T_{\mathrm{ext}}(\alpha)$ for $\lambda > 900$ nm is assumed.

Those assumptions are investigated in Section V.

III. How to Apply the Model

In this section, the steps for applying the model within device simulations are summarized. Some of the steps are optional if, for example, temperature dependence is not of interest or if the Z parameterization is undesired.

1) Determine $T_{\mathrm{ext}}(\lambda, T_0)$ and $Z(\lambda, T_0)$ for a given temperature T_0 by simulations and/or experiments.
2) Calculate $T_{\mathrm{ext}}(\alpha, T_0)$ and $Z(\alpha)$ with the same assumption for $\alpha(\lambda, T_0)$ as in Step 1.
3) Find the three Z parameters by fitting (7) to $Z(\alpha)$ for 0.6 cm^{-1} $< \alpha <$ 60 cm^{-1}.
4) For a new thickness W and temperature T_1, calculate $Z(\lambda, T_1)$ via (7) and $\alpha(\lambda, T_1)$.
5) Calculate $T_{\mathrm{ext}}(\lambda, T_1)$ by assuming $T_{\mathrm{ext}}(\lambda, T_1) = T_{\mathrm{ext}}(\lambda, T_0)$ for $\lambda < 900$ nm and $T_{\mathrm{ext}}(\alpha, T_1) = T_{\mathrm{ext}}(\alpha, T_0)$ for $\lambda > 900$ nm.
6) Calculate the generation profile $G(\zeta)$ from $T_{\mathrm{ext}}(\lambda, T_1)$, $Z(\lambda, T_1)$ and the incident spectrum $I(\lambda)$, as described in Section II-B.
7) To mitigate potentially significant numerical discretization errors: Scale $G(\zeta)$ so that $q\int_0^W G(\zeta)\,d\zeta = J_G$, where J_G is either known from Step 1 or otherwise calculated by (5).

IV. Accuracy of the Generation Profile

The model itself does not introduce any error in total generation current J_G, as this is defined via (5). Consequently, model inaccuracies can only occur by deviations of the shape of $G(\zeta)$ combined with a nonideal collection efficiency of the device. It was found in [6] that for a wide range of typical solar cell conditions the error in J_{SC} is small (< 0.1 mA/cm), by comparing simulations with the generation profile derived by ray tracing and derived by this paper's model, respectively. Here, the evaluation is extended to show the comparison with simulated EQE curves to reveal any potential significant spectral deviations.

The simulation setup is identical to [6], using a combination of the wafer ray tracer (WRT) on PV Lighthouse [10] to simulate the optics and Quokka [11] to simulate the carrier collection, wherein this paper's model is implemented as the "1-D model." The investigated device is the conventional cell of [7], altered to random pyramid texture and a specular rear reflector with a reflectance of 0.7, to be able to perform ray tracing with the WRT. It is further altered to 1-D, neglecting any front metal shading. Within Quokka, $G(\zeta)$ from the WRT is (slightly) scaled to match the actual J_G to correct for numerical errors introduced by the interpolation of $G(\zeta)$ between the different

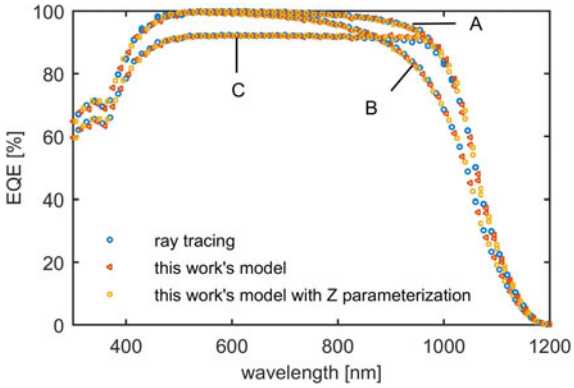

Fig. 3. Comparison of simulated EQE using this paper's model with ray tracing for three different cases A–C, as described in the study, where all cases show close agreement.

TABLE I
SUMMARY OF SIMULATED LIGHT *J–V* PARAMETERS FOR THE THREE CASES A–C AS DESCRIBED IN THE STUDY

case	V_{oc} [mV]	J_{sc} [mA/cm^2]	FF [%]	η [%]
A	638.7/638.6/638.6	40.92/40.83/40.83	81.61/81.63/81.63	21.33/21.32/21.32
B	603.8/603.6/603.6	39.25/38.89/38.89	80.78/80.84/80.84	19.14/19.01/19.01
C	633.9/633.9/633.9	38.59/38.65/38.65	81.38/81.35/81.35	19.91/19.97/19.97

The three values correspond to results obtained by ray tracing/this paper's model/this paper's model with *Z*-parameterization, respectively.

depth discretizations. EQEs are calculated by superimposing monochromatic generation profiles to a bias generation profile for three different cases: 1) using generation profiles directly from the WRT, 2) using this paper's model with T_{ext} and Z directly taken from the WRT, and 3) using this paper's model with Z parameters fitted to the former. Next to a reference case (A) with a relatively high bulk lifetime (i.e., equal electron and hole midgap SRH lifetime parameters) of 1 ms, two cases for reducing the device's collection efficiency in different ways are investigated: (B) reduction of bulk lifetime to 10 μs and (C) switching base doping to n-type, thus creating a relatively poor rear junction device due to the relatively high front and bulk recombination.

In Fig. 3, no significant error in the EQE is evident. Table I further shows that J_{SC} is the only potentially significant error in the simulated *J–V* curve. This indicates that the proposed model offers sufficient accuracy for simulating quantum efficiencies as well as *J–V* curves, even for moderately poorly collecting devices and for arbitrary spectrums. For most typical applications, experimental uncertainties and numerical errors are likely dominating, rendering the model error insignificant. For more extreme conditions, or when very high accuracy is required, an investigation of the error for the particular case should be considered.

V. EVALUATION OF THE TEMPERATURE INDEPENDENCE

A. Temperature Independence of Thin-Film Properties

To test the assumption that thin films relevant to silicon solar cells do not influence the temperature dependence of a silicon solar cell, the temperature impact on reflection of coated silicon wafers is measured. This represents the relevant influence of the thin films on solar cells more directly, as opposed to measuring their optical properties at different temperatures and modeling their impact.

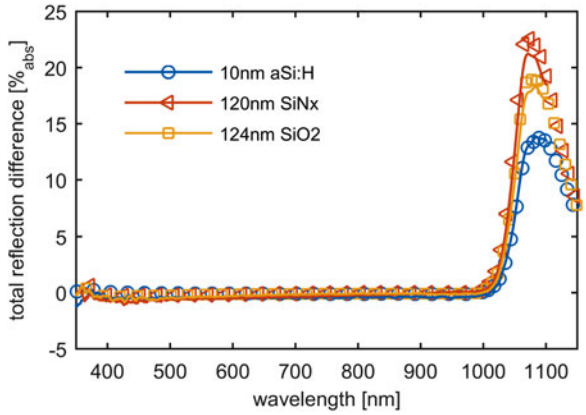

Fig. 4. Difference in total reflection between 340 and 295 K, both measured (*lines*) and modeled (*symbols*) for different thin-film materials on planar silicon samples with rear silver metallization.

Mechanically polished monocrystalline silicon samples with a thickness of 543 μm are coated symmetrically with 124 nm thermally grown SiO_2, 120 nm plasma-enhanced chemical vapor deposited (PECVD) SiN_x and 10 nm PECVD hydrogenated amorphous silicon aSi:H, and one bare sample is kept as a reference. All samples receive Ag evaporation on the rear side to increase the internal rear reflection and hence give a higher escape reflectance through the front. Total normal incidence reflection is measured using a Filmetrics F20-UV on a temperature-controlled jig at two different temperatures, 295 and 340 K. The measurements are calibrated against the bare silicon sample at 295 K.

The total reflection is modeled by using the TMM to determine internal and external reflectances and transmittances at normal incidence, and calculating a sufficiently high number of internal reflections accounting for absorption in the wafer. Temperature dependence of the complex silicon refractive index is considered using a combination of the data in [12] and [13] (where [13] is used for wavelengths not included in [12]). The optical properties of the thin films are known at room temperature either from the literature or previous experiments and are assumed to be temperature independent for the modeling.

In Fig. 4, the difference of the total reflectance between the higher and lower temperatures is shown. It can be seen that the modeling is in good agreement with the measurements, supporting the assumption of temperature independent thin-film properties. For lowly absorbing wavelengths, reflection is impacted by changes in the silicon absorption coefficient. For shorter wavelengths however, not only the thin-film properties but the resulting external reflection on silicon can be assumed to be temperature independent.

B. Validation of Other Model Assumptions Against Ray Tracing

With the assumption of temperature-independent thin-film properties, the two main remaining assumptions to be validated

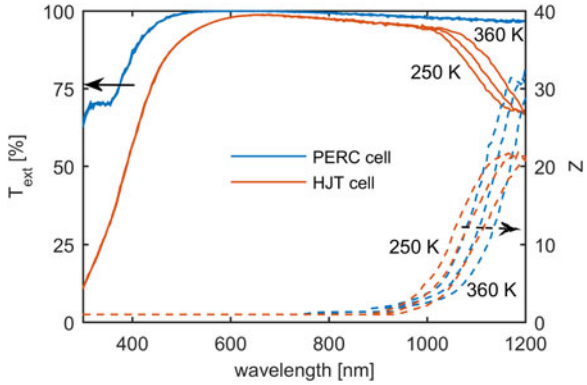

Fig. 5. T_{ext} (solid lines) and Z (dashed lines) plotted as a function of wavelength for the two considered cell types at three different temperatures (250, 300, and 360 K).

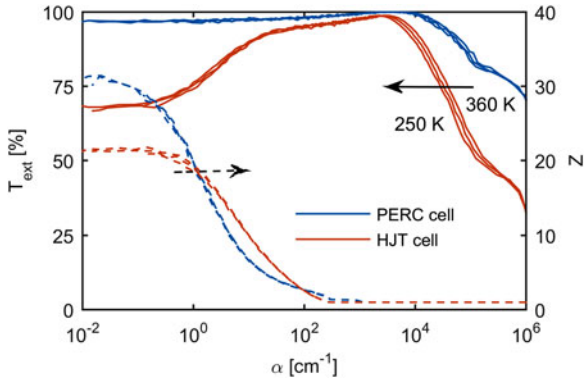

Fig. 6. Same data as above but plotted as a function of the absorption coefficient α. Note that the long wavelength region is now on the left half showing only minor temperature variations; T_{ext} at short wavelength, however, shows increased temperature variation.

are that 1) the front reflection is not impacted by the slight changes in α for highly absorbing wavelengths and that 2) the external and internal reflectances are not impacted by changes in α for lowly absorbing wavelengths. Ray tracing does not impose those assumptions and is therefore suitable for their evaluation.

For an identical device structure, ray tracing is performed with the WRT for a wide temperature range representative for solar cell operating conditions (250, 300, and 360 K). The investigated device structures are the PERC cell and the HJT cell of [7]. The PERC cell represents optical properties of typical cells in manufacturing, and better tests the aforementioned assumptions compared with the conventional cell of [7] due to its detailed optical modeling of the rear. Its properties are modified to a planar rear surface to suit the inputs of the WRT. The HJT cell presents a more challenging example due to its double side texture, as well as its more complex and more absorbing stack of thin films. Note that for the thin films of the HJT cell, in particular the TCO, it is not known whether a significant temperature dependence may exist. It should, therefore, be considered a theoretical example, which is, however, still suitable to test the aforementioned assumptions.

In Figs. 5 and 6, the results are plotted as a function of λ and α, respectively. It can clearly be seen that $Z(\alpha)$ shows only very little temperature dependence compared with $Z(\lambda)$. In addition, as expected, $T_{\mathrm{ext}}(\alpha)$ is approximately temperature

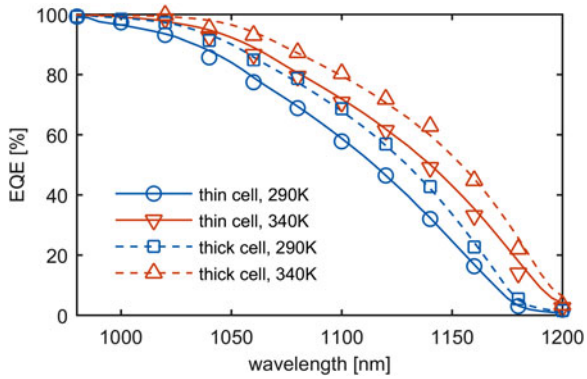

Fig. 7. Long wavelength EQE of the thick and thin IBC cell at different temperatures. *Lines*: model, *symbols*: measurements.

independent for long wavelengths and $T_{\mathrm{ext}}(\lambda)$ for short wavelengths. Notably, for the PERC cell, which represents front side optical properties for the majority of industrial silicon solar cells, $T_{\mathrm{ext}}(\lambda)$ is shown to be temperature independent for the entire spectrum.

VI. Application to Laboratory Solar Cells

Finally, the model is applied to experimental solar cells with the main purpose of testing predictive power of the underlying assumptions for changes in temperature and thickness. Two laboratory IBC cells are used. The cells are fabricated concurrently with the only controlled variation being the final thickness of the device. The starting wafer material was from the same source and thinned down for the thinner cells. The thickness of the "thin" and "thick" cell is 230 and 380 μm, respectively. The optical and electrical device properties are similar to the ones published in [14]. The EQE of each cell was measured at two temperatures (290 and 340 K), which is the minimum and the maximum temperature achievable in the experimental setup. Reflectance measurements at 300 K are combined with modeled front film absorption to derive T_{ext}.

The IBC cells have minority carrier diffusion length several times thicker than the wafer bulk and exhibit low front surface recombination, resulting in a collection efficiency $>98\%$ for the entire spectrum, as evident both from the EQE measurements and from electrical simulations. As a good approximation, an ideal collection efficiency is, therefore, assumed in the following, which simplifies the modeling largely by omitting electrical device simulations. For a known T_{ext} and Z, the EQE can then directly be calculated by

$$EQE(\lambda) = T_{\mathrm{ext}}(\lambda)\left[1 - \exp\left(-\alpha(\lambda)\, Z(\lambda) W\right)\right]. \quad (8)$$

A unique set of Z parameters is fitted to match the measured EQE of the thin cell at 290 K and is used in all subsequent calculations ($Z_0 = 31$, $Z_\infty = 1.8$, and $Z_p = 2.05$).

The measured EQEs reveal no observable temperature or width dependence up to 900 nm. This gives additional experimental evidence to the assumption of $T_{\mathrm{ext}}(\lambda)$ being independent of temperature, notably for the front side optical properties typical of silicon solar cells (silicon nitride on textured silicon). Consequently, only the long wavelength range is shown in Fig. 7.

Based on the thin cell at 290 K, to which Z was fitted, it can be seen that both the change of thickness and temperature and also their concurrent change is predicted with good accuracy. The close agreement is evidence that the model assumptions are justified on the cell level, at least for the optical properties of these particular solar cells.

VII. Conclusion

A model to rapidly calculate generation profiles from lumped optical properties, specifically applicable to wafer-based silicon solar cells, was presented. It is essentially a simplification of the established "Basore-model" by using a single lumped parameter to account for light trapping, the pathlength enhancement Z, and the external front surface transmission T_{ext}. The input parameters can be derived either from measurements of finished cells or from ray tracing or a combination thereof.

Compared with ray tracing, the derived generation profiles were shown to be sufficiently accurate for a wide range of typical silicon solar cell conditions. This includes poorly collecting devices as well as the modeling with spectral resolution, i.e., quantum efficiency simulations. Furthermore, a recently introduced parameterization of the wavelength dependence of Z was included in the investigation and was shown to not introduce additional error.

As a main benefit of the model, the input parameters are, to good approximation, independent of the incident spectrum, temperature, and device thickness, i.e., they are specific only to surface morphology and thin-film properties. The main underlying assumption of the thin-film properties showing insignificant temperature dependence was justified experimentally for three common materials. This likely holds for most other typical dielectric and metallic films used for silicon solar cells, but it should be reconsidered when using other thin-film materials (e.g., semiconductors, TCOs, etc.). Notably, for the most typical front side properties used in silicon solar cells (SiN_x on textured silicon), it was shown that T_{ext} is temperature independent for the entire spectrum relevant to c-Si solar cells.

The model was finally applied to experimental IBC solar cells and accurately predicted EQE measurements, even for a concurrent change of both device thickness and temperature.

While the model can be directly applied to model the optics of finished solar cells with appropriate optical characterization, it is useful as an extension to ray tracing: The required input parameters can be established in a single ray tracing run, which notably requires much less computational demand when not calculating the generation profile. Subsequently, the model can be used to calculate generation profiles for arbitrary spectra (e.g., quantum efficiency simulations), as well as for varying device thickness and temperature.

In particular, when integrated into an electro-optical device simulation tool, as is the case with Quokka, the model enables quantum efficiency simulations, as well as sweeping of device thickness and temperature with short computation time, high accuracy, and low user-effort.

References

[1] J. A. Rand and P. A. Basore, "Light-trapping silicon solar cells-experimental results and analysis," in *Proc. 22nd IEEE Photovoltaic Spec. Conf.*, 1991, pp. 192–197.

[2] P. A. Basore, "Extended spectral analysis of internal quantum efficiency," in *Proc. 23rd IEEE Photovoltaic Spec. Conf.*, 1993, pp. 147–152.

[3] R. Brendel, M. Hirsch, R. Plieninger, and J. Werner, "Quantum efficiency analysis of thin-layer silicon solar cells with back surface fields and optical confinement," *IEEE Trans. Electron Devices*, vol. 43, no. 7, pp. 1104–1113, Jul. 1996.

[4] S. C. Baker-Finch and K. R. McIntosh, "One-dimensional photogeneration profiles in silicon solar cells with pyramidal texture," *Prog. Photovoltaics: Res. Appl.*, vol. 20, pp. 51–61, 2012.

[5] K. R. McIntosh and S. C. Baker-Finch, "A parameterization of light trapping in wafer-based solar cells," *IEEE J. Photovoltaics*, vol. 5, no. 6, pp. 1563–1570, Nov. 2015.

[6] A. Fell and K. R. McIntosh, "Deriving the generation profile for silicon solar cells from lumped optical parameters," in *Proc. 42nd IEEE Photovoltaic Spec. Conf.*, 2015, pp. 1–5.

[7] A. Fell *et al.*, "Input parameters for the simulation of silicon solar cells in 2014," *IEEE J. Photovoltaics*, vol. 5, no. 4, pp. 1250–1263, Jul. 2015.

[8] P. A. Basore, "Numerical modeling of textured silicon solar cells using PC-1D," *IEEE Trans. Electron Devices*, vol. 37, no. 2, pp. 337–343, Feb. 1990.

[9] K. R. McIntosh *et al.*, "Quantifying the optical losses in back-contact solar cells," in *Proc. 40th Photovoltaic Spec. Conf.*, 2014, pp. 0115–0123.

[10] PV Lighthouse. (2015). [Online]. Available: http://pvlighthouse.com.au

[11] A. Fell, "A free and fast three-dimensional/two-dimensional solar cell simulator featuring conductive boundary and quasi-neutrality approximations," *IEEE Trans. Electron Devices*, vol. 60, no. 2, pp. 733–738, Feb. 2013.

[12] H. T. Nguyen, F. E. Rougieux, B. Mitchell, and D. Macdonald, "Temperature dependence of the band-band absorption coefficient in crystalline silicon from photoluminescence," *J. Appl. Phys.*, vol. 115, p. 043710, 2014.

[13] M. A. Green, "Self-consistent optical parameters of intrinsic silicon at 300 K including temperature coefficients," *Sol. Energy Mater. Sol. Cells*, vol. 92, pp. 1305–1310, 2008.

[14] E. Franklin *et al.*, "Design, fabrication and characterization of a 24.4% efficient interdigitated back contact solar cell," *Prog. Photovoltaics: Res. Appl.*, 2014, doi: 10.1002/pip.2556.

Authors' photographs and biographies not available at the time of publication.